

Optimizing the charge division Algorithm for the mini-TPC used in the tracking of the PEN experiment

Bachelor Thesis
of
Raphael Nydegger

Mathematisch-naturwissenschaftliche Fakultät
der
Universität Zürich

Prof. Dr. U. Straumann
Dr. Andries van der Schaaf
Dr. Peter Robmann

Zürich
July, 2012

Abstract

The time projection chamber (TPC) has been invented in 1971 by David Nygren and had its first major application 1981 in the PEP experiment at SLAC. So algorithms to determine the coordinates of the particle trajectories are known and well tested. With the large TPCs with anode wires of 1m or more the coordinate along a wire is determined by charge division: the charges that are received at both ends of a wire are compared to determine the coordinate.

But this algorithm fails if it is used for the mini TPC with wires of a few cm only. This thesis shows how a new algorithm which focusses on the waveform of the currents received at the two ends of an anode wire is developed and optimized. The obtained resolution of the mTPC is presented.

Contents

| | | |
|----------|---|-----------|
| 1 | Introduction | 6 |
| 1.1 | Motivation and Measurement Principles of the PEN experiment | 6 |
| 1.2 | PION decay | 7 |
| 2 | The PEN Experiment | 8 |
| 2.1 | Assembly | 8 |
| 2.2 | The mini Time Projection Chamber (mTPC) | 11 |
| 2.3 | Readout Electronics | 13 |
| 3 | The mini Time Projection Chamber analysis | 14 |
| 3.1 | The baseline subtraction | 18 |
| 3.2 | The peak search and the time measurement | 18 |
| 3.3 | The charge division algorithm | 23 |
| 3.4 | The optimization of the parameters of the algorithm | 27 |
| 4 | Results | 35 |
| 5 | Conclusion | 39 |

List of Figures

| | | |
|------|---|----|
| 1.1 | Pion decay into a positron and a neutrino | 7 |
| 2.1 | Sketch of the PEN experiment | 9 |
| 2.2 | Sketch of the central region of the experiment | 9 |
| 2.3 | Sketch of the collimator | 10 |
| 2.4 | Sketch of the mTPC | 12 |
| 2.5 | Schematic display of the mTPC | 12 |
| 2.6 | Left waveforms with baseline | 13 |
| 3.1 | Left and right waveforms of one beam particle | 15 |
| 3.2 | Left and right baseline corrected waveforms | 16 |
| 3.3 | Difference vs sum of a baseline corrected waveform | 17 |
| 3.4 | Left vs right baseline corrected waveform amplitude | 17 |
| 3.5 | Typical signals | 19 |
| 3.6 | Geometric mean of the signal amplitudes | 19 |
| 3.7 | Derivative of the signal amplitudes | 20 |
| 3.8 | Distribution of the maxima in the differentiated signals | 21 |
| 3.9 | Correlation between two adjacent peaks | 21 |
| 3.10 | Energy distribution caused by the beam particle for one wire | 22 |
| 3.11 | Summed up baseline corrected waveforms | 22 |
| 3.12 | Histogram of the original and the shifted waveforms | 23 |
| 3.13 | Differences between the mean signals for different x windows for wire 2 | 24 |
| 3.14 | Integration of the signals | 25 |
| 3.15 | Difference of the integrated signals vs time bins | 25 |
| 3.16 | Slices through 2D histogram of integrated signals | 26 |
| 3.17 | Mean x resolution vs time bin | 27 |
| 3.18 | Parameters of the algorithm (1) | 28 |
| 3.19 | Parameters of the algorithm (2) | 29 |
| 3.20 | Normalized RMS values of the collinearity test vs INTCUT2 | 31 |
| 3.21 | Two examples of the signal amplitude difference | 32 |
| 3.22 | Results for the RMS value of the collinearity tests for different set ups | 32 |
| 3.23 | Distribution of the collinearity test for a specific set up | 33 |

List of Figures

| | | |
|------|---|----|
| 3.24 | X distribution for one wire for a specific set up | 34 |
| 4.1 | X values of the algorithm vs x values of the MWPC | 36 |
| 4.2 | Distribution of the x values from the MWPC | 37 |

1 Introduction

The PEN experiment followed the PIBETA experiment which studied the $\pi^+ \rightarrow \pi^0 e^+ \nu_e$ (pion beta decay) branching ratio with the intention to determinate the CKM quark mixing matrix element V_{ud} which is the main limitation in tests of the unitarity of the CKM matrix.

The observed decay rate was normalized to the rate of $\pi^+ \rightarrow e^+ \nu_e$ decays observed simultaneously. Therefore the PIBETA already provided the experimental setup to study the $\pi^+ \rightarrow e^+ \nu_e$ decay. For the PEN experiment this setup was optimized to study the branching ratio of $\pi^+ \rightarrow e^+ \nu_e / \pi^+ \rightarrow \mu^+ \nu_\mu$.

1.1 Motivation and Measurement Principles of the PEN experiment

The $\pi^+ \rightarrow e^+ \nu_e / \pi^+ \rightarrow \mu^+ \nu_\mu$ branching ratio ($R_{e/\mu}$) is presently the best test of μe universality, i.e. the equality of the couplings of $\mu \nu_\mu$ and $e \nu_e$ to the W boson which confirms the Standard Model (SM). The experiment aims at improving the accuracy of the branching ratio by an order of magnitude [3].

If the experiment gives another result than predicted by the SM it could give insight into a W decay resulting from charged Higgs bosons [1] or decays resulting from box diagrams involving non-degenerate sleptons [2].

There are other possible contributions which will not be listed here. For more detailed information see the Annual Report of the physics institute of the university of Zurich¹.

Measurements of $R_{e/\mu}$ are based on the analysis of the e^+ energy and the time delay with respect to the stopping π^+ . The decay $\pi^+ \rightarrow e^+ \nu_e$ is characterized by $E_{e^+} = 0.5m_\pi c^2 = 69.8$ MeV and an exponential time distribution following the pion life time $\tau_\pi = 26$ ns. In the case of the $\pi^+ \rightarrow \mu^+ \nu_\mu$ decay the 4 MeV muons which have a range of about 1.4 mm in plastic scintillator can be kept inside the target and are monitored by the observation of the subsequent decay $\mu^+ \rightarrow e^+ \nu_e \bar{\nu}_\mu$ which is characterized by $E_{e^+} < 0.5m_\mu c^2 = 52.8$ MeV and a time distribution which first grows according to the pion life time and then falls with the muon life time of 2.2 μ s [3].

¹ <http://www.physik.uzh.ch/reports/report2007.shtml>

1.2 PION decay

The π^+ consists of an $u\bar{d}$ quark pair. The two quarks can combine to a virtual W^+ boson which decays into a $\mu^+\nu_\mu$ or a $e^+\nu_e$ pair. Other decays are possible but won't be mentioned here [4]

Regarding only the phase space of the two decays the decay into a positron and a neutrino is more probable than the decay into a muon and its neutrino.

From the V-A-theory of the weak interaction of charged currents we know that only left-handed particles and right-handed antiparticles are involved. The probability of the polarization of these spinors depends on the momentum which means relativistic particles have a negative helicity and relativistic antiparticle have a positive helicity [5].

For the two π^+ decays follows that the nearly massless neutrino is almost 100 % negative polarized and therefore the positron and the muon have to be also 100 % negative polarized so that the spin is conserved. Fig. (1.1) illustrates this for the rest frame of the π^+ . It is more probable for the muon to have his spin oriented opposite its flying direction than for the positron because the muon due to its higher mass has a smaller momentum. This often is called the helicity suppression of the π^+ decay.

Within the Standard Model ($g_e = g_\mu = 1$) and including the radiative corrections this leads to a branching ratio $R_{e/\mu}^{SM} = 1.2350(5) \times 10^{-4}$.

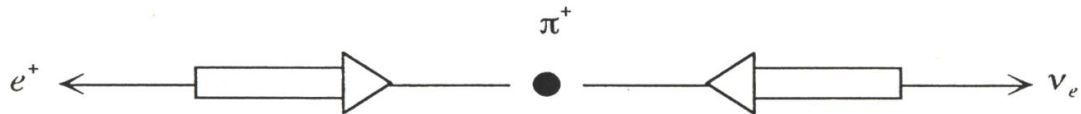


FIGURE 1.1: *Pion decay into a positron and a neutrino with the spin arrows in the rest frame of the pion.*

2 The PEN Experiment

In this chapter the assembly of the PEN experiment will be presented and the most important components will be briefly described. Only the mTPC will be discussed in more detail in section (2.2).

The PEN experiment was installed at the PSI in Villigen Switzerland. A cyclotron accelerated protons which were transported to a primary target where pions and muons were generated and transported via secondary beam lines to the experimental areas. The PEN apparatus is set up in the $\pi E1$ area with a 16 m long beam line designed to supply intense low energy pion beams with good momentum resolution. The choice of a particular beam momentum is dictated by the need for good time-of-flight separation of pions, positrons and muons between the beam counter BC (Fig. (2.3)) and the active degrader (Fig. (2.2)). The beam particles are first registered in a 2 mm thick plastic scintillator BC placed about 3 meters upstream of the lead wall (red) in Fig. (2.1). The pions are subsequently moderated in a 9 mm long active plastic degrader AD and stopped in an active plastic target AT positioned at the center of the calorimeter (Fig. (2.2)) [6].

2.1 Assembly

2.1.1 beam counter

The upstream beam counter BC is the first active detector counter mounted in the collimator Fig. (2.3). This counter tags beam particles that pass through the collimator. The central part of the beam counter is a rectangular piece of BICRON BC-400 plastic scintillator with dimensions $20 \times 10 \times 2 \text{ mm}^3$. The scintillator is optically coupled on two sides to a photomultiplier. The collimator is placed inside the vacuum pipe of the beam 4 m upstream of the active degrader. Mechanical feedthroughs at two sides of the collimator hold the magnetic shield cylinders of the PMTs [6].

2.1.2 Active Degrader

The active degrader counter is made of BICRON BC-408 plastic scintillator which has the shape of a cylinder with a diameter of 20 mm and a thickness of 9 mm [6]. A cone shaped airlight guide made of mirror foil guides the light to a PMT (see Fig. (2.4)).

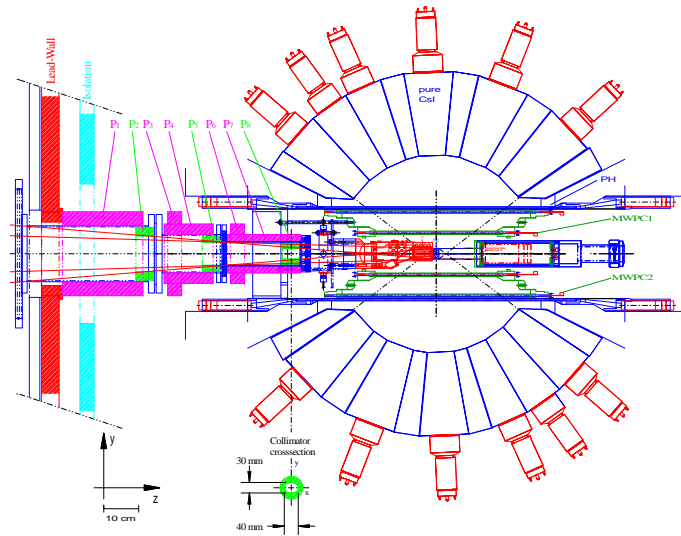


FIGURE 2.1: Sketch of the last 2m of the PEN experiment. We see how the beam is focused on the center of the calorimeter where the active target is placed.

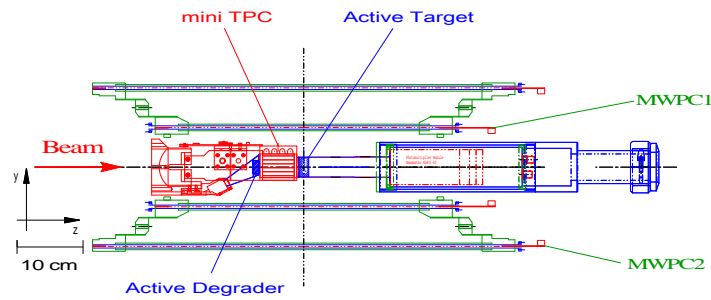


FIGURE 2.2: Central region of the experiment with Active Degradator, mTPC, Active Target and Multiwire Proportional Chambers MWPC.

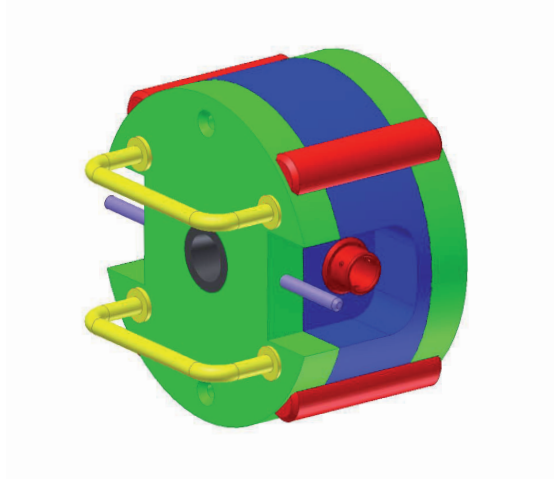


FIGURE 2.3: *Collimator made of lead and wolfram which holds the beam counter that is inserted trough the holes on the side. The diameter of the inner tube is 20 mm.*

2.1.3 Active Target

The Active Target consists of a cylindrical scintillator made of BICRON BC-422Q with 30 mm diameter and 15 mm length [6]. The target is placed along the beam axis in a cylindrical mirror foil which guides the light to a photomultiplier. In Fig. (2.2) you see the active target in the middle of the picture and to the right of it the mirror foil (violet) in front of the photomultiplier module (red).

2.1.4 Cylindrical MWPCs

Two cylindrical multiwire proportional chambers MWPC surround the active target (see Fig. (2.2)). Each chamber has one anode wire plane parallel to the z-axis and two cathode strip planes in a helical geometry. The two chambers provide a trajectory reconstruction for the decay particles [6].

2.1.5 Plastic Hodoscope

The plastic hodoscope PH is located inside the calorimeter surrounding the two concentric multiwire chambers. The hodoscope array consists of 20 independent plastic scintillator staves arranged to form a complete cylinder 598 mm long with a 132 mm radius. The scintillator light is viewed at both detector ends by two photomultiplier tubes. With the PH positrons and protons can be distinguished by their deposited energy. It additionally

delivers a good timing information (± 0.8 ns) [6].

2.1.6 Modular pure CsI calorimeter

The active volume of the shower calorimeter is made of pure Cesium Iodide. The calorimeter must cover a large solid angle and hence bears similarities to the SLAC Crystal Ball. It is made of 240 pure CsI crystals of which 220 cover the solid angle of $0.77 \times 4\pi$ sr and an additional 20 crystals cover the two detector openings for the beam entry and exit and act as electromagnetic shower leakage vetoes [6].

2.2 The mini Time Projection Chamber (mTPC)

The most important parts of the mTPC and the amplifier board will be described in this section (Fig. (2.4, 2.5)). The mTPC consists of a gas-filled chamber with 4 anode wires at a voltage of 1 kV (V_{Anode}) and a drift electrode plate at a voltage of -2 kV (V_{Drift}). The gas chamber with dimensions $40 \times 40 \times 52$ mm is continually flushed with drift gas (90% Ar and 10% C_2H_6). Seven resistors lower the the potential continually from V_{Drift} to zero (GND). This way six potentials are generated which we use for the electrodes (P1 to P6) to ensure that the electric field between the drift electrode and the anode wires (A1 to A4) is homogenous. The 40 mm long anode wires are made of nickel and chrome and have a resistance of 235Ω . Both ends of the anode wires are connected to a 10 nF capacitor. The purpose of the capacitors is to separate the high voltage of the anode wires from the voltage of the pre-amplifiers but to let pass the high frequency signal produced by the beam particle. Finally the signal is pre-amplified and conducted 20 meters to the CAEN digitizers which are described in section (2.3).

2 The PEN Experiment

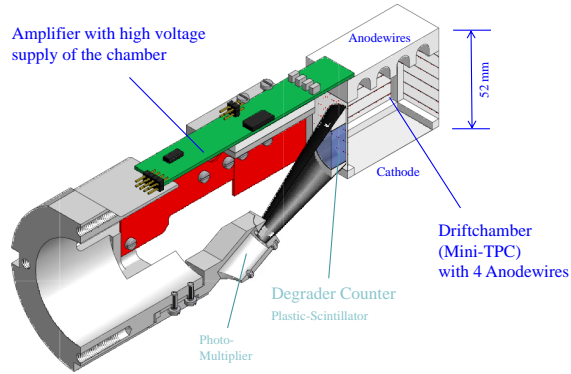


FIGURE 2.4: *The beam is coming from the left and first passes the degrader and then the mTPC. Around the plastic scintillator of the degrader counter you see the conical lightguide.*

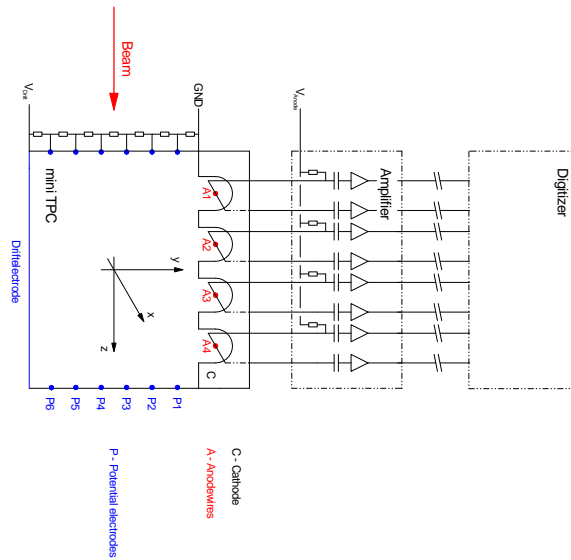


FIGURE 2.5: *Schematic display of the mTPC and the amplifier board.*

2.3 Readout Electronics

The eight signals from the left and the right end of the 4 wires are digitized with a CAEN waveform digitizer. The module has eight channels with 12 bit each. The maximal sampling frequency is 500 MHz and the maximal bandwidth is 250 MHz. The digitizer is connected by VMEbus to a computer. The digitized waveforms are stored with the help of the MIDAS software.

In Fig.(2.6) we see the left waveforms for all four wires. The maximum of the used range for recording the signals is 1024 units (10bits) with a baseline that has an uncertainty of 16 units (4bits). With that we get 6 reliable bits with which we can use to determine the position of the beam particle.

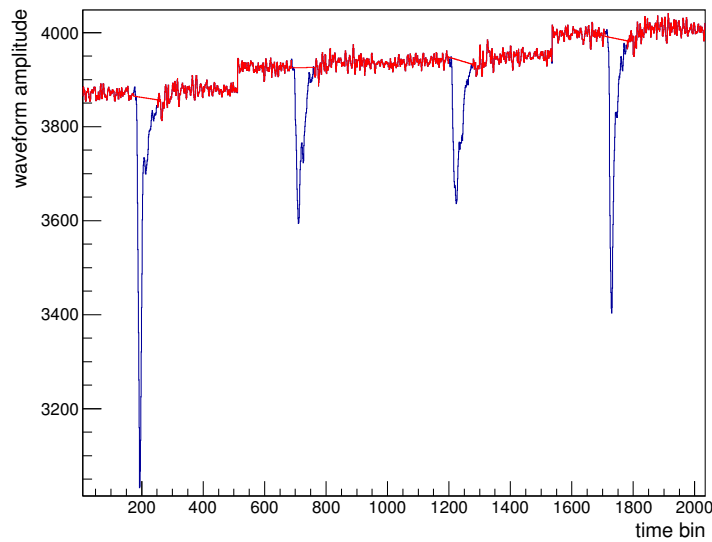


FIGURE 2.6: *The left waveforms (blue) of all 4 wires with the baseline (red) for one event. The variation in the amplitude is a result of the fluctuation in the energy loss (see Fig. (3.10)).*

3 The mini Time Projection Chamber analysis

When the PEN experiment stores an event the mini TPC signals at the left and the right end of each of the four wires are recorded. The waveforms for a typical event are shown for all four wires in Fig. (3.1).

In this example the beam particle produces a delta electron near wire 1 which we see as an afterpulse in the signal contrary to wire 2 where no delta electron was produced. Comparing the four wires one observes a steady increase in drift time which can be interpreted by an angle between the particle trajectory and the beam axis. The trigger signal for the digitizer is the same for the eight channels and is timed by the degrader counter. With this information and the drift velocity of 0.086 mm ns^{-1} the y-coordinate can be calculated where the offset must be calibrated with the help of external information (see chapter (4)).

The knowledge of the coordinate along the wires (x-coordinate) is comprised in slightly different waveforms for left and right. Due to symmetry the waveforms at both ends should look exactly the same if the particle passes in the middle of a wire. Fig.(3.2) shows the mean waveforms at different x-positions. Red was chosen for the left and blue for the right waveform. We see that the ratio of the left and the right mean waveform changes continually with the x-position. Due to slight imbalances in the readout electronic the position where the two waveforms are identical is not at $x=0.0$ but roughly at $x=1.0$.

In Fig. (3.3) the difference of the left and the right baseline corrected waveform amplitude is plotted against the sum of both baseline corrected waveform amplitudes for a particle that passes near the left end of wire 2. The integral of the sum of both baseline corrected waveforms is normalized to 1. This example shows that indeed the waveforms recorded at the left and the right end of the wire are not equal.

In Fig. (3.4) the amplitudes of many normalized waveforms are plotted against each other. The waveform amplitude in this figure is baseline corrected (= the baseline is subtracted). We see that the left and the right amplitudes are zero at the beginning and at the end of a signal. That corresponds to a situation when there is only baseline and no signal coming from ionization produced by a beam particle. While there is a signal the difference between the left and the right waveform amplitude gets bigger first and then smaller again until the signal of the beam particle vanishes. In this figure we see again that this difference depends on the x-coordinate. Our goal is now to analyze

3 The mini Time Projection Chamber analysis

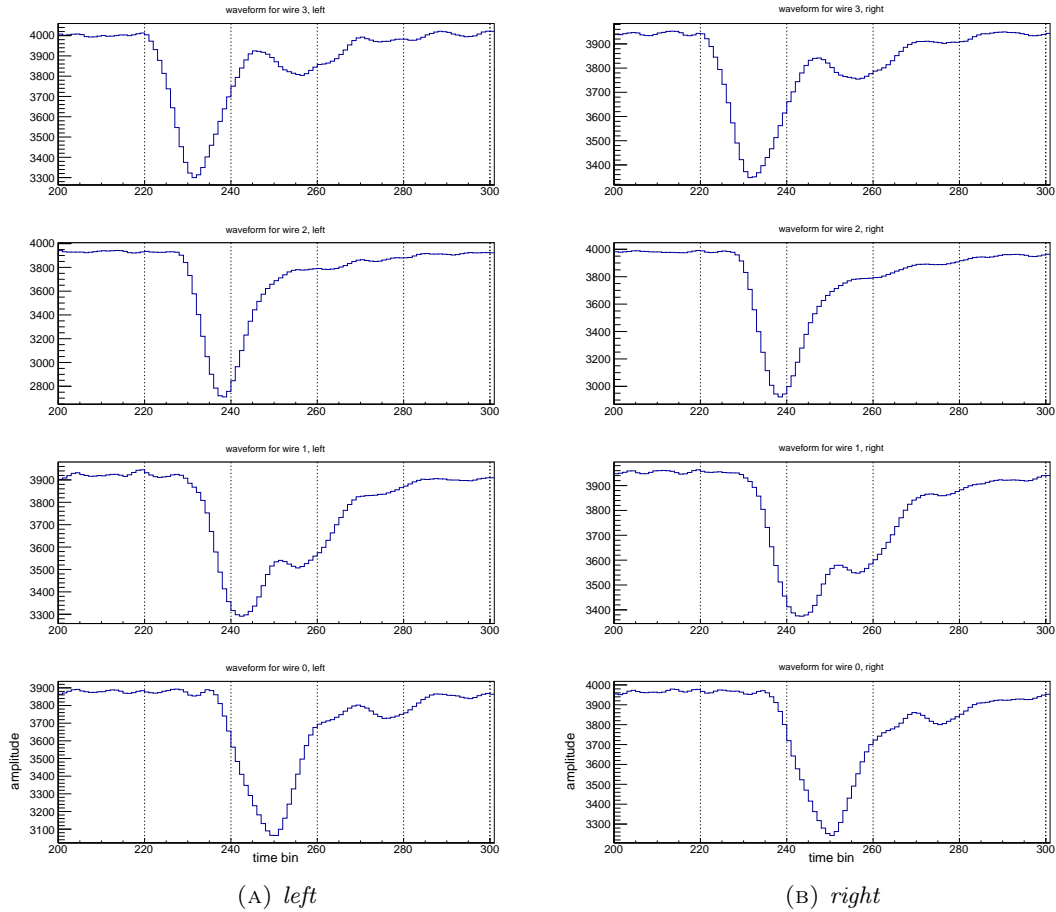


FIGURE 3.1: *The left and the right waveforms for all four wires. We see that the left and the right waveform look pretty similar. Hence the dependance on x is very subtle. The figure also shows the time shift from wire 3 to wire 0. This shift corresponds to the change in the y -coordinate. One time bin is 2 nanoseconds wide. The axes are labeled only for the lowest panels but are the same for all the other panels.*

3 The mini Time Projection Chamber analysis

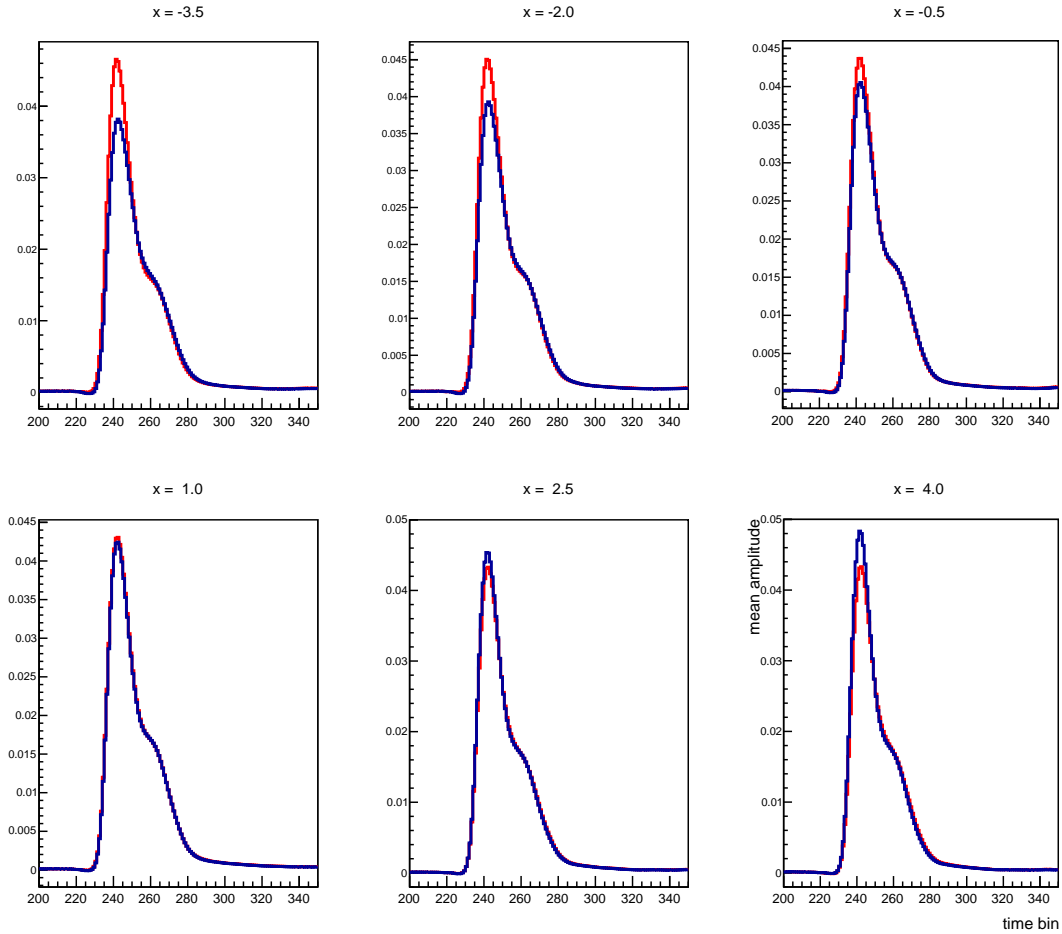


FIGURE 3.2: *The mean left (red) and right (blue) baseline corrected waveforms for different positions for wire 2. The picture shows that the difference between the waveforms continually changes with the x -position. The axes are labeled only for the last panel but are the same for all the different x windows.*

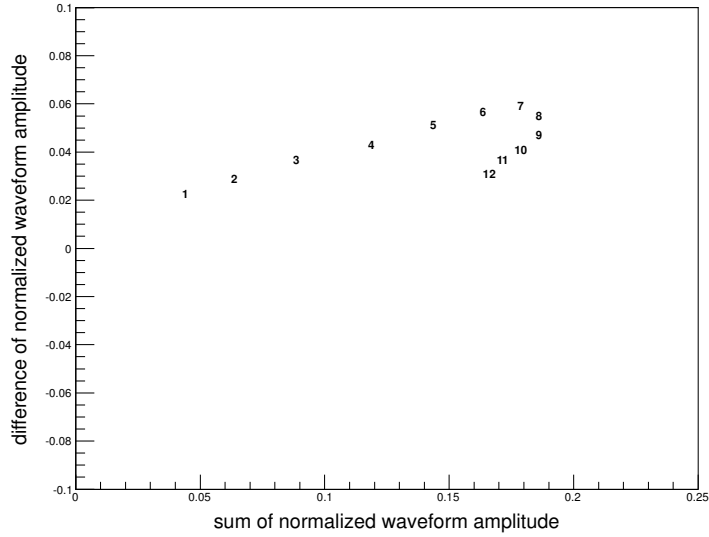


FIGURE 3.3: *The difference versus the sum of the baseline corrected waveform amplitude for 12 time bins for one event. The numbering in this figure starts with the time bin 234 and the example corresponds to the panel for $x = -3.5$ in Fig. (3.2).*

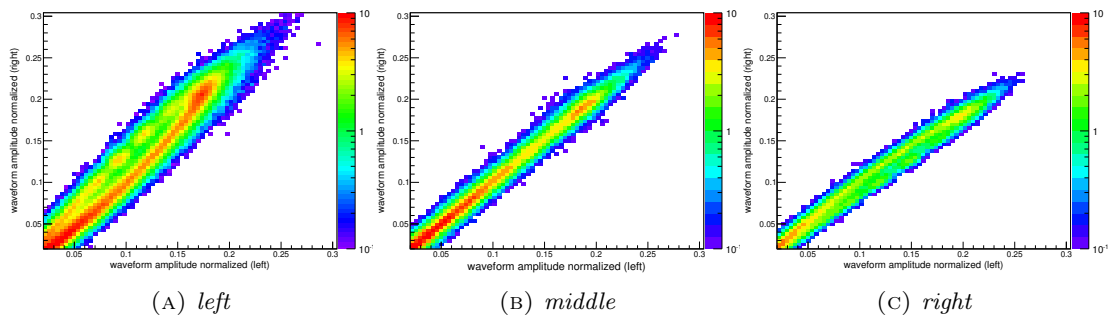


FIGURE 3.4: *Normalized right versus left baseline corrected waveform amplitude for many events. The three panels correspond to the panels for $x = -3.5$, $x = 1.0$, $x = 4.0$ in Fig. (3.2), resp.*

this dependence and develop an algorithm with the information that we get out of the recorded waveforms to determine the particle position.

In section (3.1) and (3.2) is explained how the data is analyzed. In section (3.3) is shown how the differences in the waveforms are analyzed and the algorithm is developed and in section (3.4) how the parameters of the algorithm are optimized.

3.1 The baseline subtraction

In this section we want to determine the time bins with information about a beam particle. First the left and right waveforms for all four wires are written to two histograms, one for each side (see Fig. (2.6)). Then signal regions are defined either because the value of the amplitude is lower than 3600 or because the difference of two neighbouring amplitude values (slope) is larger than +5 or lower than -5 (see Fig. (3.18)).

Then the mean amplitude (= mean baseline) of the baseline regions (!= signal regions) is calculated separately for each wire. Time bins of the original waveform with values which are a minimum distance away from the mean baseline of the corresponding wire are identified as signal regions.

The next step is to delete signal regions which are narrower than 10 time bins. All other signal regions are enlarged by 5 time bins left and 20 time bins right.

Now only the values of the time bins of the baseline regions are copied from the original waveform and written to a new histogram. Two neighbouring loose ends of the baseline regions have to be connected (see Fig. (2.6)). For that purpose the mean value of the 14 time bins next to a loose end is calculated separately for both loose ends. These two values are used to connect the the two time bins next to a gap in the baseline by linear interpolation.

With these preparations we can now fill a histogram with only the signals of the original waveforms by subtracting the baseline values (red) from the original waveform values (blue) and multiplying the result by -1. This is done for waveforms recorded at the left and the right end of each wire. Fig. (3.5) shows the left and right signals of all four wires for one event.

3.2 The peak search and the time measurement

Our next goal is to find the two neighbouring signal amplitudes with the largest difference between them (= steepest slope) in each signal and to determine the corresponding time bin. For this purpose the signals for left and right (Fig. (3.5)) are now combined by taking the geometric mean (see Fig. (3.6)). Negative signal values are set to zero. To find the largest slope the geometric mean of the two signals is differentiated and searched for maxima (see Fig (3.7)). The time bin with the largest value is called time bin of the recognized peak TIK (see Fig. (3.18))

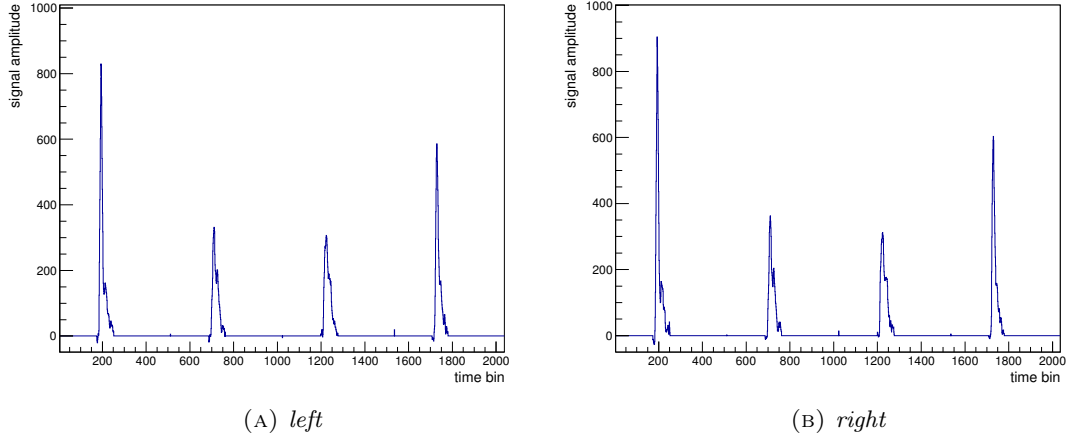


FIGURE 3.5: *Typical signals for all wires.*

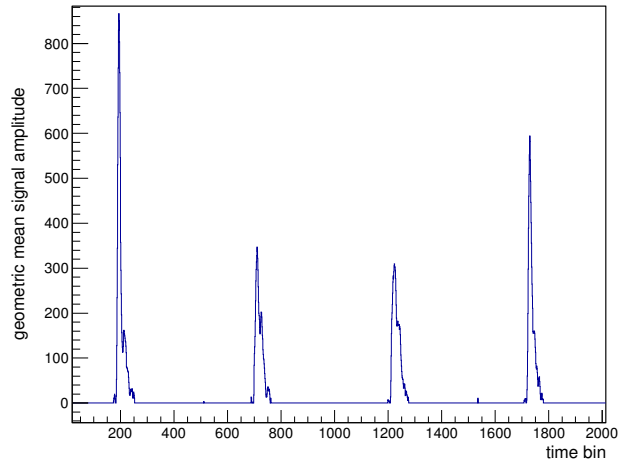


FIGURE 3.6: *The geometric mean of the left and the right signal amplitude. Negative entries in the signal amplitude have been set to zero.*

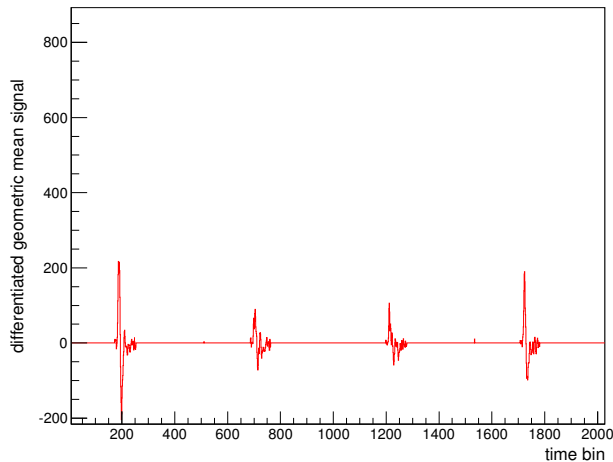


FIGURE 3.7: *The derivative of the geometric mean of the left and right signal amplitude.*

A peak with its corresponding time bin TIK is accepted if it fulfills the following criteria:

- The maximum in the differentiated signal is larger than a certain value. This criterium is used to suppress maxima which are caused by a noise signal. Fig. (3.8a) shows all local maxima and Fig. (3.8b) the absolute maximum for many events. In a typical event a signal has one peak and hence the differentiated signal has one maximum with a large value. But if there is a fluctuation in the ionization (see wire 1 in Fig. (3.1)) or a fluctuation in the baseline which is falsely interpreted as a signal other maxima with smaller values are found in the differentiated signal.
- The actual peak is uncorrelated with the peak found before. A correlation between two peaks indicates that they belong to the same particle crossing. In Fig. (3.9) we see a correlation between the time difference and the energy difference of two neighbouring peaks. We suppress peaks which appear within 80 time bins and differ less than 500 in deposited energy from the proceeding peak.
- The signal covers a minimum area. Since the covered area scales with the amount of the ionization caused by the beam particle it is called deposited energy. We see in Fig. (3.10) that there are no signals with deposited energies less than 500 that have to be taken into account.
- The drift time varies over a range that is defined by the maximal drift path of about 12 mm. We see in Fig. (3.11) that the variation of the time signal correlation

with the trigger is confined to time bin 180 to 320.

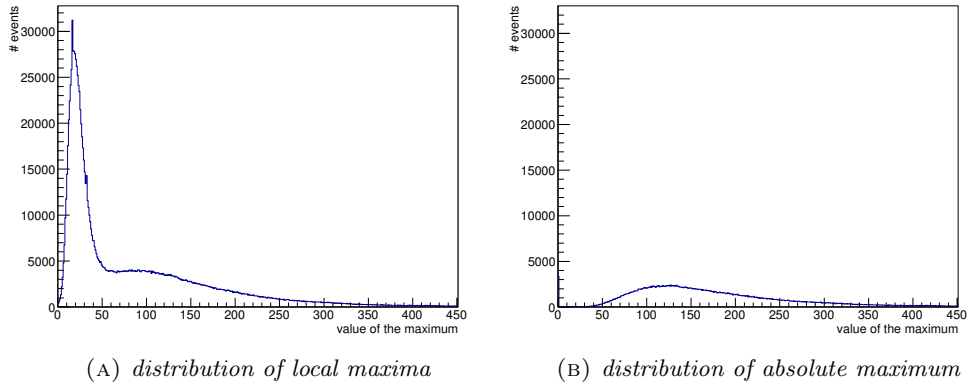


FIGURE 3.8: *Distribution of the local maxima and the absolute maximum in the differentiated signal.*

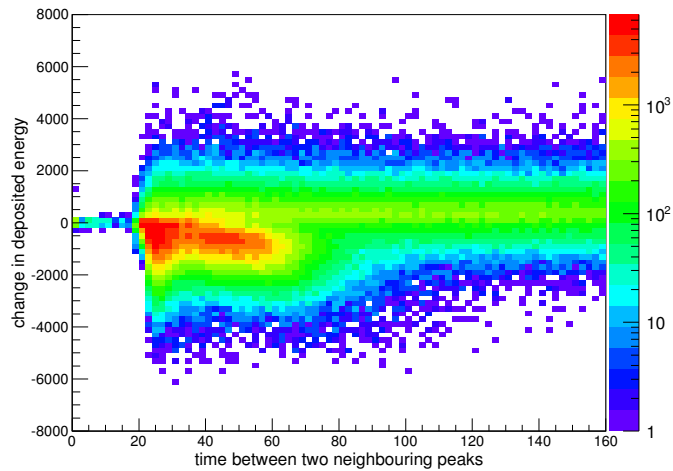


FIGURE 3.9: *Correlation between two adjacent peaks: the change in the deposited energy of two neighbouring peaks in a signal versus the time between the neighbouring peaks in the same signal. For time below time bin 70 one observes an enhancement caused by afterpulses. The region below time bin 20 is empty since the algorithm requires a minimum separation.*

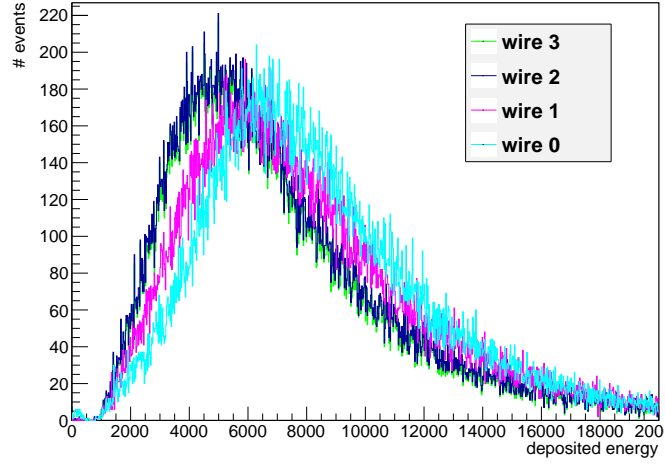


FIGURE 3.10: *Distribution of the deposited energy (= area covered by a signal) in the mTPC for all four wires.*

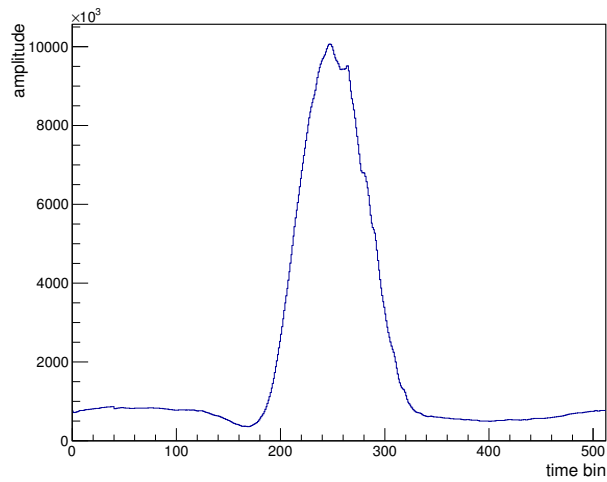


FIGURE 3.11: *The summed up waveforms of many events. The signals caused by the beam particles lay between time bin 180 and 320.*

3.3 The charge division algorithm

The waveform depends on the distribution of the ionization along the about 10 mm track element and on the space coordinates of that track element.

The energy loss per wire varies as can be seen in Fig. (3.10) and (2.6). Hence if two beam particle pass at the same x-coordinate they can cause two differently scaled waveforms and the algorithm must not depend on that. To avoid such problems the waveforms are normalized to the sum of the left and the right signal values.

The next goal is to make the waveform drift time independent and then to study a mean signal from particles which passed in the same window of the x-coordinate. The final goal is the analysis of the difference between the signals at the left and the right end of a wire with the purpose to reconstruct the position in x. The x values that are used to select the waveforms of the particles are calculated with the old charge division algorithm.

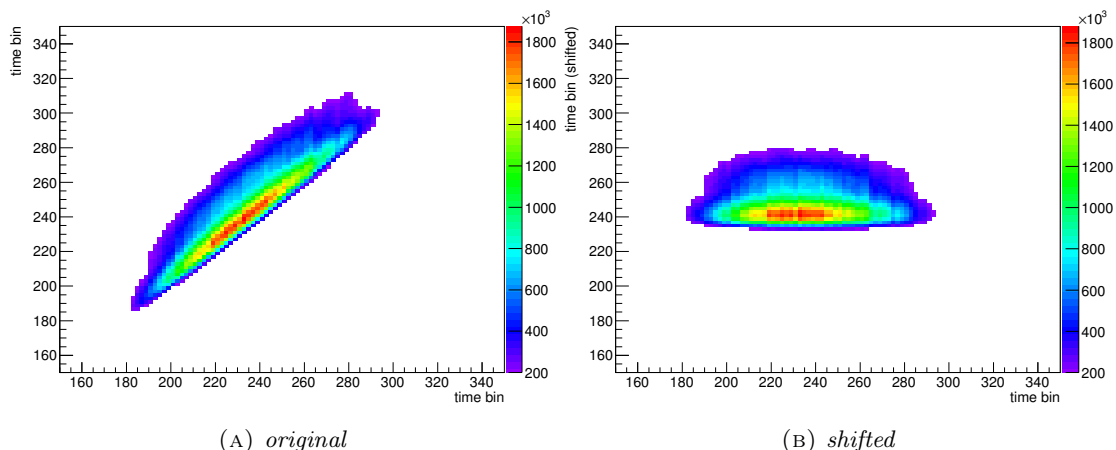


FIGURE 3.12: *2D histogram of the original and the time shifted waveforms versus the peak position. On the y-axis are the time bins of the corresponding waveform with the waveform amplitude along the z-axis. The time bin of an accepted peak is arbitrarily set to time bin 235 for the shifted time bins (y-axis in the right panel).*

To make the waveforms time independent they have been shifted to the time of the observed peak. In Fig. (3.12) the time dependent waveforms are shown left and the time independent waveforms are shown right. The time for all accepted peaks has been set arbitrarily to time bin 235.

In Fig. (3.13) we see the differences of the mean signals for seven windows in the x-position set with the old algorithm. During our analysis we want to quantify these

differences and therefore as a first step sum up the signal values starting with the first time bin of a signal. This bin is defined by the parameter SLOPELEFT which is shown in Fig. (3.18).

The results of these summations are shown for one event with two waveform peaks in Fig. (3.14b). In time bin 1800 we see the result of the summation of the signal amplitude from time bin 1773 to 1800, in time bin 1801 we see the sum from 1773 to 1801 and so on. But doing so we have to pay attention at waveforms containing two signals. For such situations it is important that the integral (summation) is set to zero at the beginning of a signal so that for waveforms with two signals the two integrals are separated (see figure(3.14)).

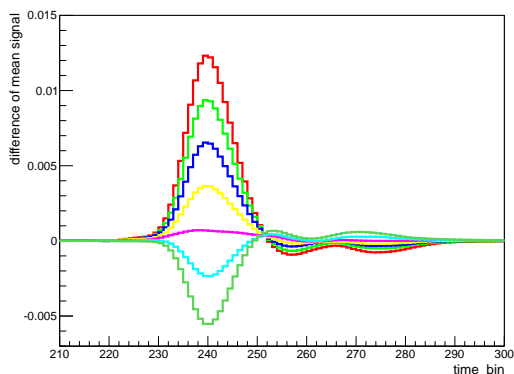


FIGURE 3.13: Mean left signal minus mean right signal for wire 2. Mean signal means the normalized signal for many events. The different colors correspond to different x windows set with the old charge division algorithm. The x coordinate axis is set to zero in the middle of the anode wires.

Constraining the data to waveforms with only one observed peak made the analysis easier and I worked for a while with only these events. For many events the difference of the integrated signals for left and right is calculated and plotted in a 2D histogram. This is done for several windows on the x -coordinate-axis (see Fig. (3.15)). With a rootmacro the histograms of several runs (which means a lot more statistics) are summed up and finally slices through these 2D histograms along the y -axis at different time bins are made and displayed one above the other in Fig. (3.16).

With the help of these plots one can study until which time bin one has to integrate to separate the different x -positions best. So we can now say that for a fix integration time bin and a fix x -coordinate the width of the observed peaks in Fig. (3.16) divided by their separation is a measure of the position resolution.

In Fig. (3.17) we see the dependence of the resolution on the final time bin used for

3 The mini Time Projection Chamber analysis

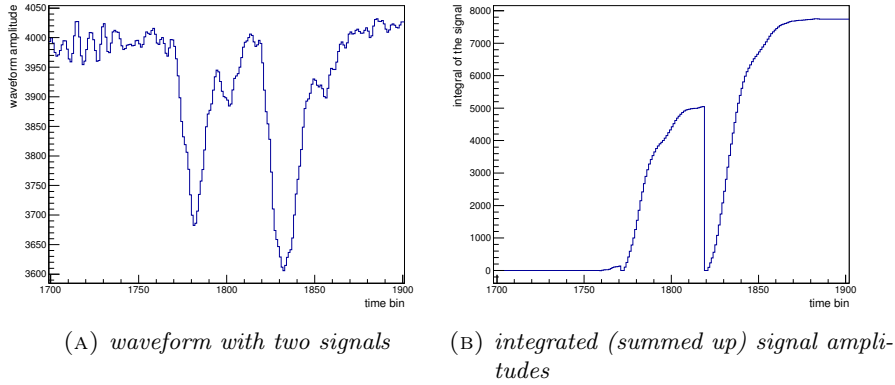


FIGURE 3.14: Integration of the signals: For each signal the values of the time bins are summed up starting at the lowest bin. This starting bin can be varied by changing the *SLOPELEFT* parameter. Example: In the figure we see that the integral of the first signal is set to zero at time bin 1773. Hence in bin 1780 we have the sum from bin 1773 up to bin 1780. For the second signal the summation starts at bin 1882.

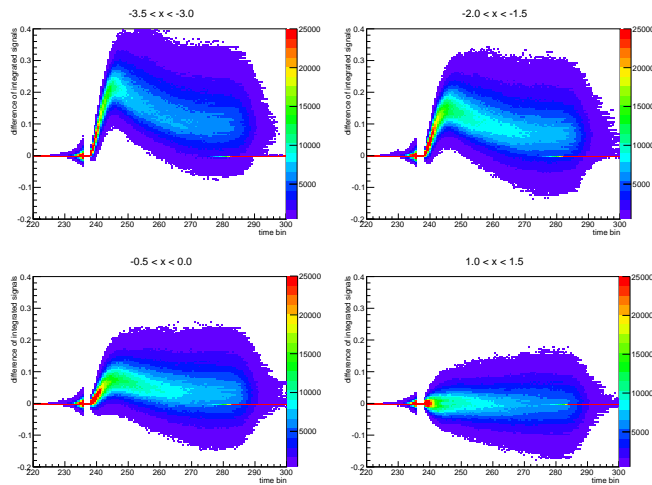


FIGURE 3.15: The difference of the integrated signals versus the time bin. See Fig.(3.14b) for information about the integration of the signal. The integrated signal at the right end of the wire was subtracted from the one from the left end. The four panels belong to different x windows.

3 The mini Time Projection Chamber analysis

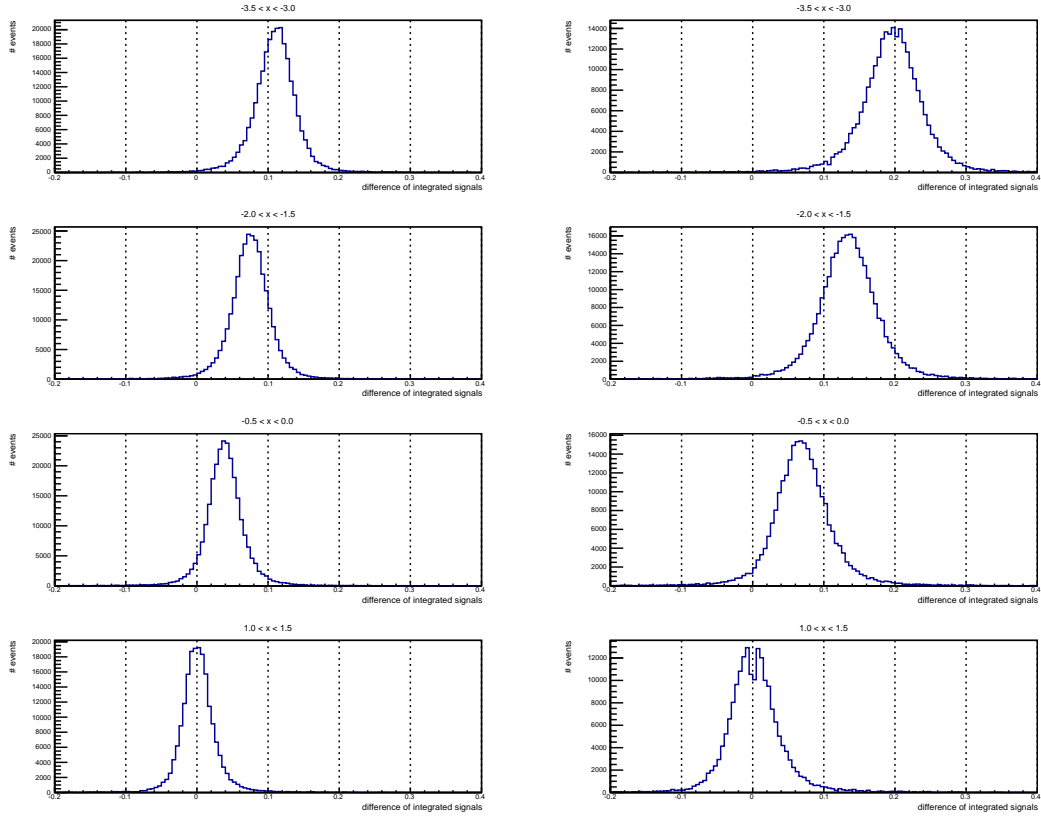


FIGURE 3.16: Slices through all 4 histograms in Fig. (3.15) at time bin 240 and 245. We see that the summation of the signal amplitudes up to time bin 245 separates the x -windows better than the summation up to time bin 240.

the summation of the signal difference amplitude.

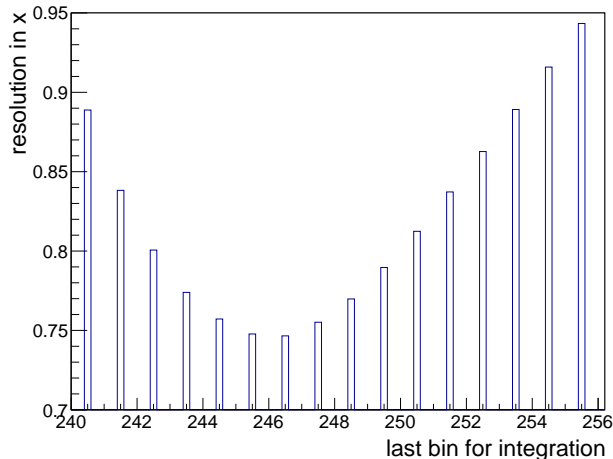


FIGURE 3.17: Mean x -resolution versus the time bin where the summation of the difference of the signal amplitude ends.

With all these preparations we have now developed an algorithm that searches for signals in a recorded waveform, then finds peaks in the signals and compares the left signal with the right signal and integrates the difference for a certain time span to determine the x -coordinate. In the next section we will discuss how these algorithm can be optimized.

3.4 The optimization of the parameters of the algorithm

The numerical values of the different parameters of the present algorithm have been optimized as will be described in this section. The problem with the present method of choosing the final time bin which is discussed in the previous section is its dependance on the old algorithm.

The old algorithm is used to select the events for the different x -windows. It would be better to have a test which is independent of the old method.

A collinearity test would be such kind of test because the beam particle moves along a straight trajectory through the mTPC (see equation (3.1) and (3.2)). So ignoring scattering and assuming perfect reconstruction we would get zero for every collinearity test. The lower the result of our collinearity test, the better our position algorithm. If the x coordinate of a wire has a wrong offset the mean value of the collinearity test is not zero even if the algorithm works perfectly well. A good measurement of the accuracy is the RMS value of the collinearity test which is not affected by this shift. The lower the RMS value the better the algorithm.

Figure (3.18) shows the various parameters used in the algorithm and after the figure follows a list of these parameters, their optimal value and a short explanation.

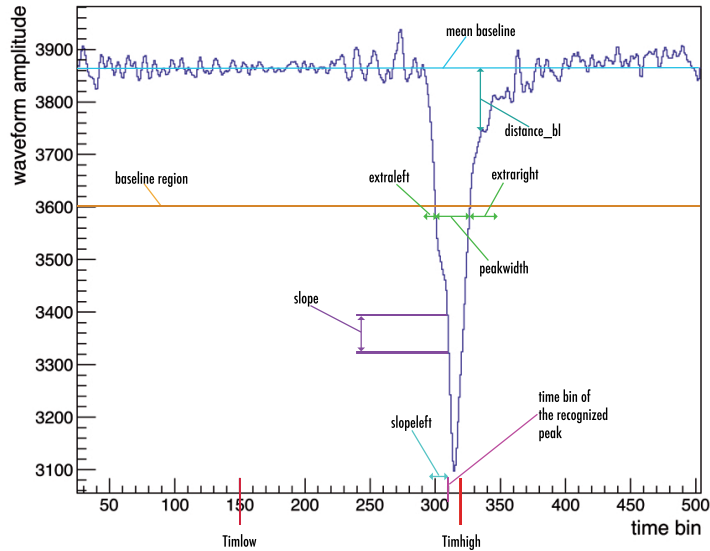


FIGURE 3.18: *The parameters of the algorithm shown in the picture of a typical waveform.*

- **baseline region** = 3600: Waveform values that are lower than the baseline region are recognized as signal region.
- **slope** = 5: Difference between two neighbouring waveform values. If this difference is larger than +5 or smaller than -5 the containing time bin is added to the signal region.
- **distance_bl** = 50: Distance to the mean baseline. Time bins which contain waveform values that have a larger distance to the mean baseline than `distance_bl` are added to the signal region.
- **peakwidth** = 15: Minimum width of a signal region.
- **extraleft** = 5, **extraright** = 20: Number of time bins which are added left and right to the bins of an accepted signal region.
- **time bin of recognized peak (TIK)**: TIK is set to the bin in an accepted signal region with the steepest slope. It is called peak because we search for a peak in

the differentiated signal amplitude as it is explained in section (3.2) and showed in Fig. (3.6) and (3.7).

- **Timlow** = 150: Sets a lower bound for TIK.
- **Timhigh** = 320: Sets an upper bound for TIK.

There are other parameters not shown in Fig. (3.18) to suppress afterpulses (which you see in Fig. (3.9)) and eliminate fluctuations in the baseline that means signals with only little deposited energy.

The most important parameters for optimizing the resolution of the algorithm are shown in Fig. (3.19) and listed below with a short explanation.

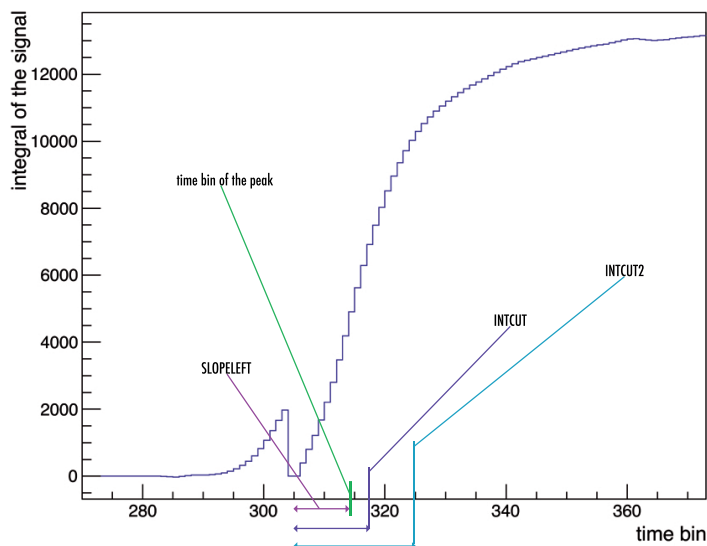


FIGURE 3.19: *The most important parameters for optimizing the resolution of the algorithm shown in the picture of an typical integrated signal.*

- **INTCUT** Defines the time bin where the summation of the signal values ends. To this sum value the signal is normalized.
- **INTCUT2** Defines the time bin where the summation of the signal difference ends.
- **SLOPELEFT** Defines how many time bins before the TIK the integral is set to zero.

- **INTERPOLATE** Defines how many neighbouring time bins are used for the interpolation. The interpolation between two loose ends of the baseline is explained in section (3.1) and showed in Fig. (2.6).

The formulae for the two collinearity tests that are used to compare the new algorithm with the old one are listed below:

$$\text{collinearity test 1} = x_1 + x_2 - x_0 - x_3 \tag{3.1}$$

$$\text{collinearity test 2} = x_1 + x_2 - (x_0 - x_3) \times \frac{1}{3} \tag{3.2}$$

An important parameter is INTERPOLATE which defines how many neighbouring time bins are used for the interpolation of the baseline in a signal region (see Fig. (2.6)). Finally the best results are reached if the 14 channels next to the left and right end of a baseline region are used to calculate the mean value for the interpolation.

The optimal values of many parameters are correlated. For example if the normalization is changed, the optimal time bin to end the summation of the signal difference changes too. In other words if INTCUT is varied the optimal value for INTCUT2 changes.

Hence we vary the two parameters together and calculate the collinearity test. This is done for many events. Finally the RMS value of the collinearity test distribution is normalized to the average of the RMS values of the corresponding four x distributions (see Fig. (3.23 and (3.24)). Later in this chapter will be explained in more detail why this is done. Now we can write these results into a histogram and search for the lowest value.

An example how the RMS value of the collinearity tests changes if the two parameters are varied is shown in Fig. (3.20). For the variation a new variable delta is created and INTCUT is set to INTCUT2 + delta with the intention to get more informative figures. The delta variable is varied from -10 to + 30 and the INTCUT2 variable from 30 to 69. So Fig. (3.20) does not show the uninteresting lower part of the INTCUT2 variation for two fix delta values.

We can see that the optimal INTCUT2 value for delta = -1 is different than for delta = +5. The optimal value changes from 43 in Fig. (3.20a) to 47 in Fig. (3.20b).

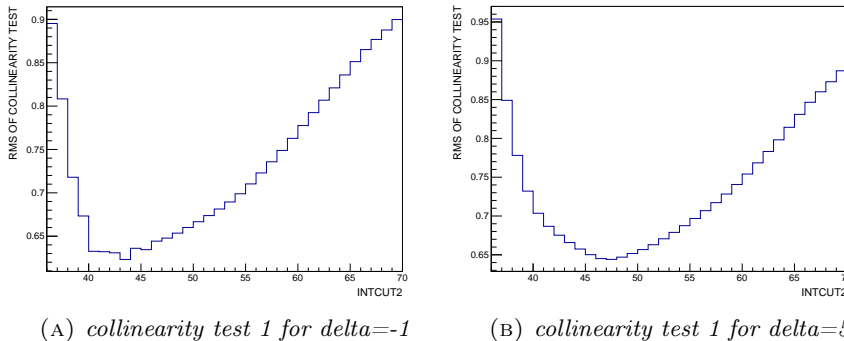


FIGURE 3.20: The normalized RMS values of the collinearity test versus the time bin where the summation of the signal difference ends (= INTCUT2). For each set up the RMS value of the collinearity test distribution (many events) is normalized to the average of the RMS values of the corresponding four x-distributions. The INTCUT parameter is set to INTCUT2 + delta.

Another important parameter is SLOPELEFT. In Fig. (3.14) is shown how the sum of the signal difference is set to zero at the beginning of a signal. SLOPELEFT defines where exactly the summation starts.

To further optimize the algorithm the before discussed parameters have to be varied with different SLOPELEFT values. To see which SLOPELEFT values could be candidates for the best value we take a look at Fig. (3.21). In this figure the difference between the shifted signal amplitude arriving at the left and the right end of a wire in the mTPC is shown for one event in each panel.

The TIK of the two signal differences is set to 235. This choice was arbitrarily made and also discussed in chapter (3.3). Starting at time bin 220 we see that the amplitude of the signal difference is wobbling at the beginning before it starts showing a clear peak about time bin 230 and finally is going back wobbling around zero. Therefore it seems plausible that the best RMS values have been found with SLOPELEFT = 5.

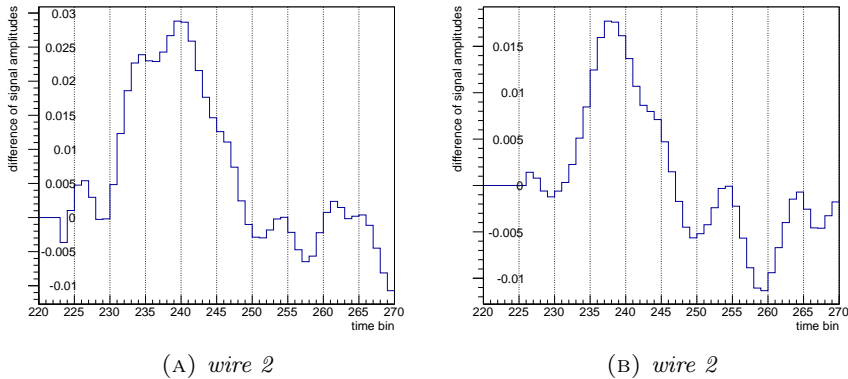


FIGURE 3.21: The figure shows two examples of the difference of the right and the left signal amplitude of one event. It helps finding the best value for the *SLOPELEFT* parameter which defines where the summation of signal difference values starts.

In Fig. (3.22) we see the best results for the normalized RMS values of both collinearity tests. Both collinearity tests give the lowest RMS value with $\delta = -3$. For the collinearity test 1 the optimal *INTCUT2* value is 42 and for the collinearity test 2 the optimal value is 43.

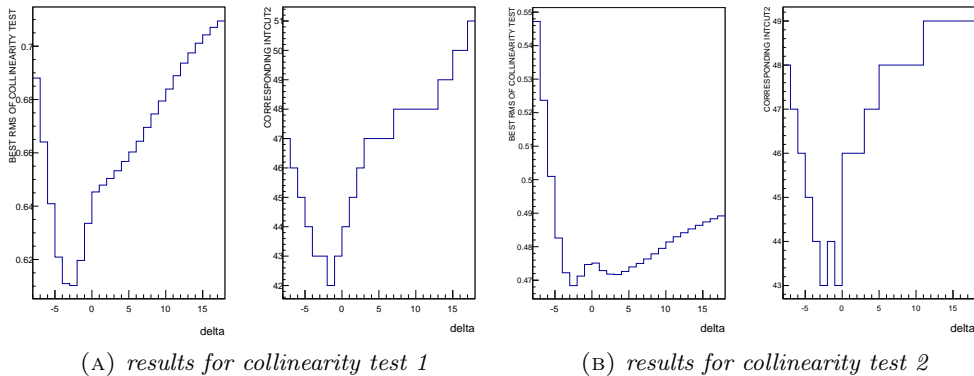


FIGURE 3.22: The left panel shows the best RMS value for a specific set up and the right panel shows the corresponding *INTCUT2* parameter. The *INTCUT* parameter can be calculated with the formula $INTCUT = INTCUT2 + \delta$. All RMS values are normalized to the average RMS of the corresponding *x*-distributions.

The final goal is to improve the algorithm and therefore the results of the collinearity tests for both algorithms have to be compared. To do so the x values are calculated with the old and the new method for several runs. That gives the possibility to plot the x-distributions (see Fig.(3.24))and the distributions of the collinearity tests (see Fig.(3.23)) which finally give a direct comparison between the old and the new algorithm.

The problem with comparing the RMS values of the collinearity tests of two different set ups is that they are dependent on the x distributions. The wider the x distributions of the four wires, the larger the RMS of the collinearity tests. One solution for this problem would be to make a calibration for the x values and to calculate the collinearity tests with the same units for the different set ups.

Another solution is to take into account the not calibrated x distributions and to normalize the collinearity tests to the average width (average RMS) of these distributions. This way the results are not calibrated absolutely but relatively to each other which fulfills the purpose to compare them for different set ups.

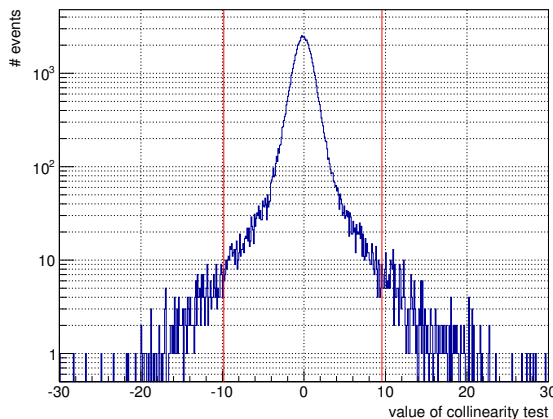


FIGURE 3.23: *Distribution of the collinearity test values for one specific set up. The results that have less than 10 entries (1 %) are cut off. The two vertical red lines mark this cut. This way collinearity test values that are influenced by scattering are suppressed. The RMS value that is used to determine the resolution is taken from the constrained figure.*

Comparing the new with the old algorithm shows that the new one is 25 % better (see Table(4.1)). So the new algorithm works pretty nicely but there is no evident physical reason why the information taken from the left and the right signal should be a 100 % good up to a certain channel and suddenly useless after this channel. That is what is done actually with optimizing the INTCUT2 parameter.

Another approach is not to cut the information from 100 % to 0 % from one time bin

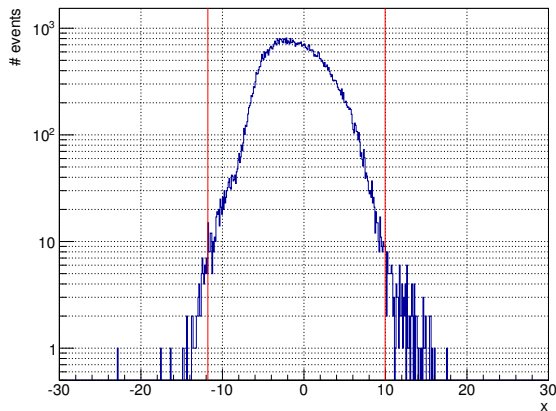


FIGURE 3.24: *Distribution of the x values for one wire and one specific set up. The results that have less than 10 entries (1 %) are cut off. The two vertical red lines mark this cut. This way x values that are influenced by scattering are suppressed. The RMS value that is used to determine the resolution is taken from the constrained figure.*

to another but to weight the values of the different time bins with a triangle function and to set the information used for the integration continuously to zero. This way the aforementioned problem would be avoided. The function which is used to weight the values doesn't have to be a triangle function. The most important demand to the function is that the first time bin of the signal difference has most and the last has no weight.

Optimizing this newly introduced function it came clear that the INTCUT and INTCUT2 optimization had become useless, because with the new parameters the sum of the signal difference became constant before the normalization and the integration time bin had been reached.

With the new approach the SLOPELEFT and the new created WIDTHMAX parameter became the most important ones considering the resolution of the algorithm. After varying them to optimize the resolution they are set to: $SLOPELEFT = 2$ and $WIDTHMAX = SLOPELEFT + 15$. With that a better resolution as with the old approach has been reached. The results of the normalized collinearity tests are shown in Tab. (4.1) and finally an improvement of 44 % has been reached.

4 Results

In the table (4.1) below the normalized RMS values of the collinearity tests are listed. As it is explained in the previous chapter the different algorithms can be compared this way. The lower the RMS value the better the algorithm.

All these results have not yet been calibrated absolutely. To calibrate the mTPC we use two multi wire proportional chambers (MWPCs) and combine the trajectory of a pion with the trajectory of a positron. The positron results from the pion decay which is explained in detail in section (1.2).

The two MWPCs are concentric cylinders arranged around the target (see Fig. (2.2)). The wire spacing of the MWPCs is 2 mm and the diameter of outer MWPC is the double of the inner one. For vertical trajectories the x value is constant and given by:

$$x_{MWPC} = 2 \times x_{inner} - x_{outer} \quad (4.1)$$

Therefore we select only decay positrons which are emitted within $\pm 10^\circ$ from the vertical direction. Finally the x values of the two trajectories are plotted in Fig. (4.1).

TABLE 4.1: *The normalized RMS values of the results of the collinearity tests. The algorithm has been steadily optimized until finally there has been an improvement of 43 % for the algorithm with the triangle function.*

| collinearity test | test 1 | test 2 | average | improvement factor |
|--------------------------------------|--------|--------|---------|--------------------|
| old algorithm | 0.827 | 0.598 | 0.713 | 1.0 |
| new algorithm | 0.602 | 0.461 | 0.532 | 0.75 |
| new algorithm with triangle function | 0.465 | 0.346 | 0.406 | 0.57 |

If both detectors are calibrated the slope of the distribution (red line) would be 1.0 and with the right offset it would pass through 0.0. Since the offset does not affect the collinearity tests it is here neglected.

If the slope of the distribution is 1.0 also the RMS values of the projection onto the x and the y axis are the same. The projections onto the y axis are already known. They are nothing else than the x distributions that have been used earlier. The only thing that is left to do is to project the distribution on to the x axis, suppress the bins with less than 10 entries as was done with the others and get the RMS value of the distribution (see Fig. (4.2)). We can now multiply our results with this RMS value and our resolution is calibrated absolutely. The RMS is 4.175 mm and we get the absolutely calibrated results shown in Tab. (4.2).

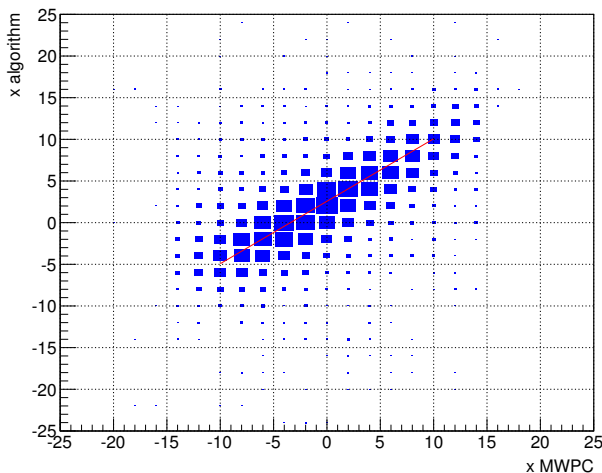


FIGURE 4.1: *2D plot of the x values from the algorithm and the x values from the MWPCs. The slope of the red line is 0.75. For a calibrated algorithm the slope would be 1.0. The offset can be determined as well.*

With the formulae for the collinearity tests (3.1) and (3.2) and the errors (RMS values) from table (4.2) the error in x can be calculated. Hence the x resolution of the algorithms can be calculated. Table (4.3) shows the absolutely calibrated resolutions for all three discussed algorithms. The achieved relative resolution of the mTPC with an anode wire length of 0.04 m is 2.4 %.

Other detectors as the Prototype of the Straw Tube Tracker used in the PANDA experiment achieved a similar resolution. The time dependent charge asymmetry algorithm that was used to determine the position along the anode wire of 1.52 m length had a relative resolution of about 2 % for particles with the same energy as the pions in the

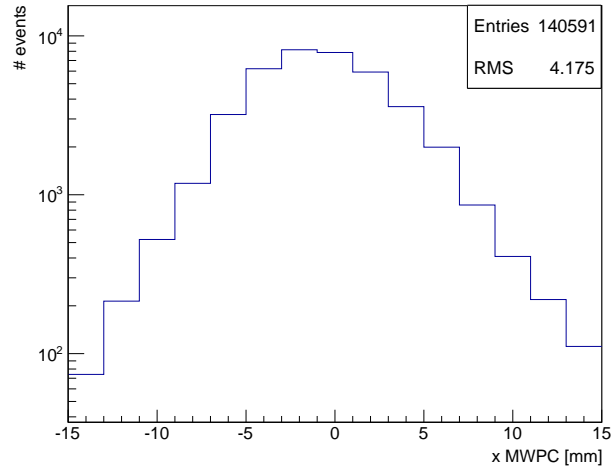


FIGURE 4.2: *The projection of Fig. (4.1) onto the x axis. After suppression of the bins with less than 10 entries results a RMS value of 4.175 mm.*

TABLE 4.2: *The absolutely calibrated RMS values of the results of the collinearity tests.*

| collinearity test | test 1 [mm] | test 2 [mm] | average [mm] | improvement factor |
|---|----------------|----------------|-----------------|--------------------|
| old algorithm | 3.45 | 2.50 | 2.98 | 1.0 |
| new algorithm | 2.51 | 1.93 | 2.22 | 0.75 |
| new algorithm with triangle function | 1.94 | 1.45 | 1.69 | 0.57 |

4 Results

TABLE 4.3: *The absolutely calibrated errors on the x values calculated with the errors of the two collinearity tests for the different algorithms. In the fourth column Δx is the average error and L is the length of the anode wire of the $mTPC$.*

| error on x with | test 1 [mm] | test 2 [mm] | average [mm] | $\Delta x/L$ [%] | improvement factor |
|---|----------------|----------------|-----------------|---------------------|--------------------|
| old algorithm | 1.73 | 1.68 | 1.71 | 4.3 | 1.0 |
| new algorithm | 1.26 | 1.29 | 1.28 | 3.2 | 0.75 |
| new algorithm with triangle function | 0.97 | 0.97 | 0.97 | 2.4 | 0.57 |

PEN experiment[7]. This algorithm optimizes the longitudinal resolution by taking into account the different propagation times for the signals received at the left and the right end of a wire.

5 Conclusion

It has been an interesting project which provided me deep insight into the analysis of waveforms. Most time has been invested in learning how waveform analysis works including how to use ROOT¹. Another focus has been on the variation of the correlated parameters which has been quite tricky sometimes. The outcome of the optimization of the algorithm was a success and I am satisfied with the result of my work.

All this time I worked with the data of one day of 2009 which was split into several runs each of them covering 20 minutes. It would have been nice to see if my work helps to improve the calibration of the mTPC for the whole year of 2009 and 2010 which is done now while I am writing my thesis by the group from Dubna (Russia).

¹ A data analysis software developed at CERN

Bibliography

- [1] J. h. Park, JHEP **0610** (2006) 077.
- [2] M. J. Ramsey-Musolf and S. Su, *Low energy precision test of supersymmetry*, arXiv:hep-ph/0612057.
- [3] P. Robmann et al., *A precision determination of the $\pi^+ \rightarrow e^+\nu$ branching ratio*, Annual Report 2006/07, University Zurich, (2007).
- [4] C. Amsler et al. (Particle Data Group), PL B667, 1 (2008) and 2009 partial update for the 2010 edition (URL: <http://pdg.lbl.gov>)
- [5] C. Amsler, *Kern- und Teilchenphysik*, vdf Hochschulverlag AG, ETH Zürich, (2007).
- [6] E. Frlez et al., *Design, Commissioning and Performance of the PIBETA Detector at PSI*, arXiv:hep-ex/0312017 v1, (2003)
- [7] A. Sokolov et al., *Application of the time-dependent charge asymmetry method for longitudinal position determination in prototype proportional chambers for the PANDA experiment*, Nuclear Instruments and Methods in Physics Research A 574 (2007) 50-56